NANO
LETTERS

XXXX
Vol. xx, No. x
-

Super-Resolution without Evanescent Waves

Fu Min Huang and Nikolay I. Zheludev*

Optoelectronics Research Centre, University of Southampton SO17 1BJ, United Kingdom

Received January 20, 2009

ABSTRACT

The past decade has seen numerous efforts to achieve imaging resolution beyond that of the Abbe−Rayleigh diffraction limit. The main direction of research aiming to break this limit seeks to exploit the evanescent components containing fine detail of the electromagnetic field distribution at the immediate proximity of the object. Here, we propose a solution that removes the need for evanescent fields. The object being imaged or stimulated with subwavelength accuracy does not need to be in the immediate proximity of the superlens or field concentrator: an optical mask can be designed that creates constructive interference of waves known as superoscillation, leading to a subwavelength focus of prescribed size and shape in a field of view beyond the evanescent fields, when illuminated by a monochromatic wave. Moreover, we demonstrate that such a mask may be used not only as a focusing device but also as a super-resolution imaging device.

The past decade has seen numerous efforts to achieve imaging resolution beyond that of the Abbe−Rayleigh diffraction limit, which proscribes the visualization of features smaller than about half of the wavelength of light with optical instruments. The main direction of research aiming to break this limit seeks to exploit the evanescent components containing fine detail of the electromagnetic field distribution. Indeed, many powerful concepts such as scanning near-field optical microscopy (SNOM)[1,2] and the use of various forms of field concentrators[3−6] and superlenses[7−13] depend on the exploitation or recovery of evanescent fields. The proper far-field optical superlens[7] requires bulk negative index materials that are still to be developed, while other designs, though offering substantial advances, are united by a common severe limitation: that the object being imaged or stimulated must be in the immediate proximity of the superlens or field concentrator. Here, we propose a solution that removes this limitation: an optical mask can be designed that creates constructive interference of waves known as superoscillation, leading to a subwavelength focus of prescribed size and shape in a field of view beyond the evanescent fields, when illuminated by a monochromatic wave. Moreover, we demonstrate that such a mask may be used not only as a focusing device but also as a super-resolution imaging device.

In fact, in his seminal 1952 paper Toraldo Di Francia demonstrated that propagating waves can create subwavelength localization of light in the far-field with the suggestion of a pupil design providing an accurately tailored subwavelength diffraction spot using a series of concentric apertures.[14] Such a subwavelength concentrator could be employed as a focusing device in a super-resolution scanning optical microscope where the object is placed several wavelengths away from the device, thus removing the main limitation of near-field instruments. More recently, Berry and Popescu,[15] starting from earlier works on quantum mechanics, showed that diffraction on a grating structure could create subwavelength localizations of light that propagate further into the far field than more familiar evanescent waves. They relate this effect to the fact that band-limited functions are able to oscillate arbitrarily faster than the highest Fourier components they contain, a phenomenon now known as superoscillation.[16−18] Examples of subwavelength localizations of light generated by a nanohole array[19,20] and a thin meta-dielectric shell[21] have been demonstrated recently. Research on beating the diffraction limit actually has an even longer history: in 1922, Oseen, with reference to Einstein's radiation needle stick, proved that a substantial fraction of the emitted electromagnetic energy can be sent into an arbitrarily small solid angle.[22] Beginning from the pioneering work of Shelkunoff,[23] the microwave community contemplated the idea of achieving antennae that beat the diffraction limit for directivity: several authors were able to prove that for a linear array of properly adjusted radiating antenna dipoles, there were no theoretical limits to directivity whatsoever.[24,25] However, the sharp increase in the proportion of reactive to radiated power that would be required to achieve superdirectivity means that the antenna gain increase is offset by the need to provide an even higher increase in the power to the antenna to maintain the signal level, thus rendering the concept of superdirective antennae impractical. As we will see below, achieving a subwavelength localization of light in the far-field also comes at a price of losing most of the optical energy into diffuse sidebands. Nevertheless, optical

10.1021/nl9002014 CCC: $40.75

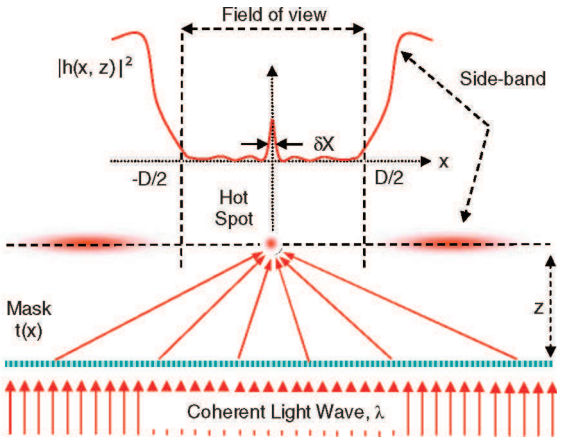

Figure 1. Optical superoscillation. An arbitrary field distribution with an arbitrarily small hot-spot δx, within a limited area $[-D/2, D/2]$, can be generated by diffraction of a plane electromagnetic wave from a purposely designed mask.

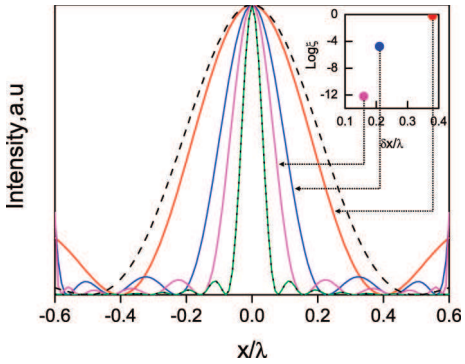

Figure 2. Normalized intensity profiles for a hot-spot with $\delta x = 0.07\lambda$ (black dotted line) and its approximations by series of bandwidth-limited prolate spheroidal wave functions $|h(x)|^2$ truncated at $N = 2$ (red line, $\delta x_2 = 0.38\lambda$); $N = 6$ (blue line, $\delta x_6 = 0.21\lambda$); $N = 10$ (pink line, $\delta x_{10} = 0.14\lambda$); and $N = 26$ (green line overlapping with the black dotted line, $\delta x_{26} = 0.07\lambda$). The dashed line shows the $\lambda/2$ limit for a hot-spot achievable with a high-numerical aperture cylindrical lens. Insert: Energy (ξ) contained within the hot-spot as a function of its size (δx).

microscopy applications can tolerate much higher losses than those acceptable in antenna design: scanning microscopes can work with only a few photons per second, giving one around 18 orders of magnitude of power reserve (assuming that a 1 W laser is used as the optical source).

In this letter we make a further step in the investigation of the potential of superoscillation for imaging and achieving subwavelength foci. We derive an algorithm for designing a mask that creates a subwavelength focus of prescribed size and shape within a prescribed field of view when illuminated by a monochromatic wave. Moreover, we show that such a mask may be used not only as a focusing device but also as a super-resolution imaging tool. We also study the role of manufacturing imperfections on the achievable super-resolution and suggest a design for a superoscillation plasmonic energy concentrator.

The typical situation that we address here is presented in Figure 1: we aim to design a mask, which, within a limited area $[-D/2, D/2]$ (field of view), will create a small hot-spot of light concentration (superoscillation) with a width δx located outside the evanescent zone, at a distance $z > \lambda$ from the mask, where λ is the wavelength of light illuminating the mask. We argue that in principle a mask can be designed to create a hot-spot that is arbitrarily small, with an arbitrary profile, located at any given distance from the mask.

Our consideration is limited to a one-dimensional mask $t(x)$ creating a one-dimensional subwavelength field distribution $h(x)$ (superoscillation) when illuminated by a plane wave at wavelength λ, although generalization to a two-dimensional case is trivial. The desired superoscillation feature located at a distance from the near-field zone of the mask can only be created by diffraction on the mask if the feature can be decomposed into a series of plane waves with wavevector $|k_0| = (2\pi)/(\lambda)$. Therefore, the main step in designing the mask is to present the desired superoscillating field as a series of bandwidth limited functions that can be decomposed into free-space plane waves of the given wavelength λ. We argue that *any* arbitrary small field feature can be presented as a series of *band-limited* functions if we are concerned with a prescribed field of view $[-D/2, D/2]$. This may be achieved using the formulizm of prolate spheroidal wave functions developed by Slepian and Pollark[26] to treat problems of information compression. This is a complete set of functions orthogonal in the interval $[-D/2, D/2]$ and across the whole range $[-\infty,\infty]$. The main feature of prolate spheroidal wave functions is that they are *band-limited* to a frequency domain $[-k_0, k_0]$. Therefore the mask design algorithm comprises the following steps: initially, the desired subwavelength hot-spot is presented as a series of prolate spheroidal wave functions, which can be truncated when a satisfactory level of approximation is achieved; at the second step, this series of prolate spheroidal wave functions is presented as a series of plane waves, and, using the scalar angular spectrum description of light propagating from the mask to the superoscillating feature, the required complex mask transmission function $t(x)$ can be readily derived. The formulizm of the algorithm is presented in the Appendix.

In what follows, we will give an explicit example of a mask designed to generate a subwavelength concentration of light. Let us aim for a single hot-spot field distribution $Sinc(ax/\lambda)$ centered in the field of view $[-D/2, D/2]$. The full-width-at-half-maximum δx of the intensity profile of this distribution is measured as $2.784\lambda/a$. From now on, we will set $a = 40$, aiming therefore to achieve a $\delta x = 0.07\lambda$ hot spot in a $D = 1.2\lambda$ field of view, far beyond the Abbe−Rayleigh limit. Figure 2 shows the intensity profile of this distribution alongside a number of consecutive approximations to the distribution formed by a limited series of prolate spheroidal wave functions and a curve representing the Abbe−Rayleigh limit that would be achievable by a cylindrical lens with unitary numerical aperture. One can see that the series rapidly converges and that when $N = 26$ the width of the approximation is practically the same as that of the target field distribution.

Figure 3 shows the intensity $|t(x)|^2$ and phase φ profiles of the mask $t(x) = |t(x)|e^{i\varphi}$ required to create the field profile corresponding to $N = 6$, which has $\delta x = 0.21\lambda$, at a distance

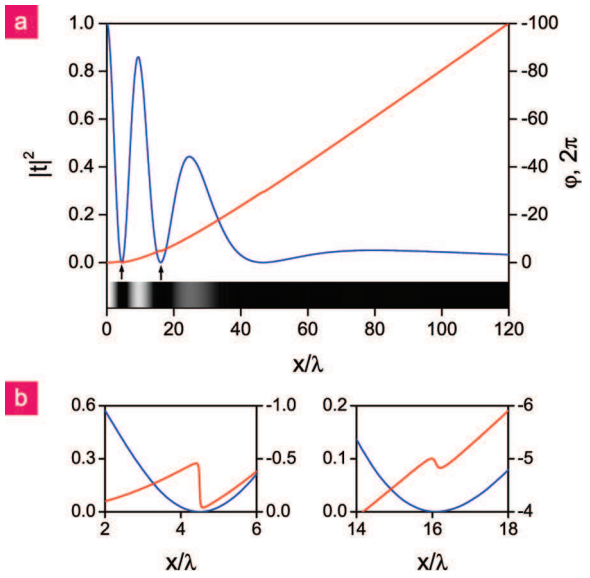

Figure 3. Mask profile for the generation of a subwavelength hot-spot. (a) Intensity $|t(x)|^2$ (blue line) and phase $\varphi(x)$ (red line) profiles of the mask transmission function $t(x)$, which generates a hot-spot with $\delta x = 0.21\lambda$ at a distance $z = 20\lambda$ from the grating. At the bottom, a gray scale map of the intensity profile is also presented. (b) Close-up detail of kinks in the phase curve at the points highlighted with arrows in a.

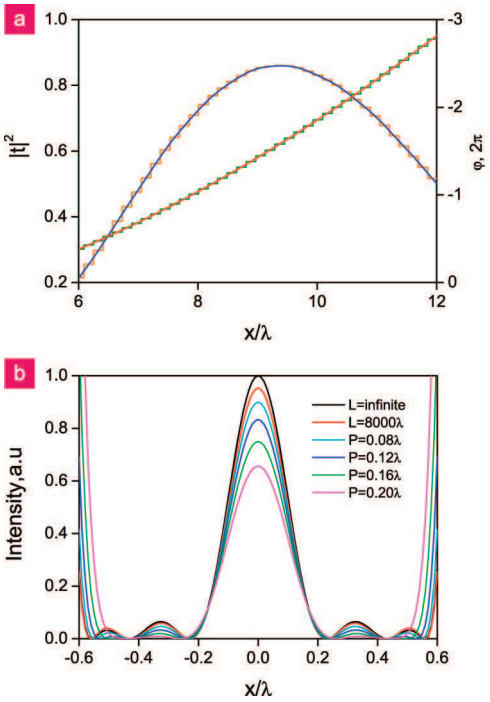

Figure 4. Role of finite mask length and manufacturing imperfections on mask performance. (a) Intensity and phase characteristics of an ideal mask (smooth lines) and its stepped equivalent, where the step of 0.16λ mimics the manufacturing pixelation. (b) Calculated intensity profiles of hot-spots generated by an ideal infinitely long mask (black line); an ideal mask truncated to a length of 8000λ (red line); and 8000λ long masks pixelated to 0.08λ (cyan line), 0.12λ (blue line), 0.16λ (green line), and 0.2λ (pink line).

$z = 20\lambda$ from the grating. As the mask transmission function is even, only part of profile for $x \geq 0$ is shown here. One can see that there is a small central area $[-40\lambda, 40\lambda]$ of the mask that transmits most of light. Beyond that area, there is a low-intensity broad shoulder of a slowly fading transmission characteristic. The phase profile of the mask resembles that of a concave lens where the optical thickness is at a minimum in the center. The monotonous increase is only interrupted at a few positions where transmission amplitude is close to zero (indicated by arrows) and the phase shows a kink as illustrated in the zoomed sections (b).

The superoscillation process is based on the precise and delicate interference of waves; therefore, we investigated its stability with respect to the manufacturing tolerances to which masks can be fabricated and to the need to use masks of finite length (see the description of the practical device design below). We found that for the mask presented in Figure 3, an 8000λ long device may be used instead of an infinitely long mask without any substantial degradation of performance ($\delta x = 0.21\lambda$ for both infinite and truncated masks with a 5% intensity decrease for the finite mask). A practical mask is likely to be manufactured by electron-beam lithography or focused ion-beam milling with a certain limited resolution; therefore, we also investigated the dependence of superoscillation hot-spot size and intensity on the pixelation of the grating design: we replaced the smooth transmission function with stepped functions in which the step width corresponded to the resolution P of the manufacturing process (see Figure 4a). Figure 4b shows the variation of the intensity profile with increasing pixelation. The superoscillation process is remarkably stable against this manufacturing imperfection: with pixel size increasing to 0.2λ, the δx width of the hot-spot only increases by about 8%. Pixelation has a more substantial influence on the peak intensity, which is reduced by about 40% under such conditions.

To quantitatively characterize the optical energy contained in a superoscillating hot-spot, we define ξ as the ratio between the energy contained in the hot-spot (between the first intensity minima either side of the central peak) and the total energy transmitted through the mask. In the inset to Figure 2, we show values of ξ against the width of the peak δx for different levels of approximation $N = 2, 6, 10$. One can clearly see that the smaller the hot-spot is, the lower the proportion of energy that goes into it. For example, for $N = 6$ only 1.74×10^{-5} of the total transmitted energy will be focused into the hot-spot. The energy contained in the hot-spot is also significantly dependent on the field of view: if the required field of view is decreased by a factor of 2 from $D = 1.2\lambda$ to $D = 0.6\lambda$, the proportion of energy going into the hot-spot at $N = 6$ increases by nearly 3 orders of magnitude to 4.8×10^{-2}. In fact, a more general consideration of the superoscillating functions shows that the intensity in the hot-spot may only decrease polynomially with its width.[17] We therefore argue that when designing practical realizations of superoscillating masks, less demanding requirements on the shape of hot-spots may yield much higher values of ξ. Moreover, one may achieve much higher values of ξ for a given size of hot-spot by relaxing the requirements on the field structure of the hot-spot pedestal (the background level within the field of view), for instance by stipulating

only the maximum field intensity in the pedestal area relative to that of the hot-spot, but not the exact profile of the pedestal.

Recently, we have shown theoretically and experimentally that a hole array can be used as an imaging device.[27] Similarly, a superoscillating mask can also be designed to image a subwavelength object. In wave optics, a conventional lens focuses a wavefront via a gradual change of the phase delay, leading to an interference-driven convergence of radiation into a focus. The ability of the mask to image has similar origin as it creates a precisely tailored superposition of waves, leading to an interference-driven superoscillatory convergence into a hot-spot. The ability of the mask to focus may be characterized in terms of effective numerical aperture NA_{eff}. Indeed, a conventional cylindrical lens in vacuum focuses a plane wave into a line with width of $0.5\lambda/NA$ where NA is the numerical aperture of the lens. Thus, a mask corresponding to a series of prolate spheroidal wave functions truncated at $N = 2$ that will focus a plane wave into a 0.76 λ line has an effective numerical aperture of $NA_{eff} = 1.38$. For comparison, using specialized oil-immersion glass lenses it is possible to achieve $NA \approx 1.4$, while the highest possible value of the numerical aperture of a conventional lens in vacuum is $NA = 1$. For the mask corresponding to $N = 6$, 10, and 26, effective numerical apertures are $NA_{eff} = 2.38$, 3.57, and 7.14, correspondingly, that are completely out of reach for conventional optics. Moreover, a mask can be designed to image a narrow slit source on one side of the mask into a subwavelength line image on the other side of the mask. Our simulation of the field structure on the imaging side of the mask indicates that it creates a single imaging plane, at a distance prescribed by a design procedure. Such a mask performs the function of a cylindrical lens: when the slit source moves along the plane of the mask, its image moves in the opposite direction. Here when the source is displaced, the precise superposition of the diffracting wave changes, creating a displaced image that remains subwavelength in width. We have shown that such a line-to-line mask images two closely spaced optical slit sources into two line images with a resolution exceeding that of a conventional cylindrical lens. This is illustrated in Figure 5, where we present a mask with a transmission function that converts a line source located 20λ from the mask to a subwavelength line image on the opposite side of the mask, also at 20λ, thus performing the function of a cylindrical lens (see eq A6 of the Appendix). Such a lens offers a subwavelength resolution: Figure 5b illustrates the imaging of two incoherent slit sources (each 0.04λ wide) separated by a distance of 0.24λ. Here, the image on the slits is clearly resolved according to the Rayleigh criterion,[28] which states that the total intensity at the saddle point of the sum intensity profile of two just-resolved slit sources is 81% of the maximum intensity. Resolving two slits indicated that the mask should be able to image an incoherently illuminated object of high complexity. The mask can also be used for super-resolution scanning imaging application when the object is scanned against the mask within the field of view, while the light on the opposite side of the mask is collected through a subwavelength aperture.

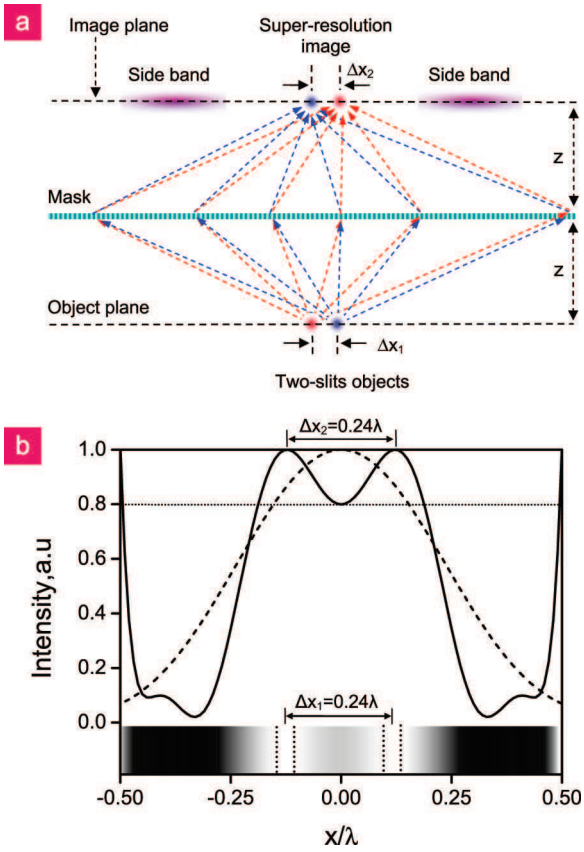

Figure 5. (a) Superoscillation mask as a subwavelength imaging device. (b) Intensity profile of the image of two subwavelength slits separated by a distance $\Delta x_1 = 0.24\lambda$, located at a distance 20λ from the mask. The intensity distribution is also shown in gray scale at the bottom of the image where the dotted lines indicate the positions of the two slits. For comparison, the dashed line shows the intensity profile of the image field of the two slits as imaged by a conventional cylindrical lens with unitary numerical aperture and a resolution of $\lambda/2$.

In comparison with conventional near-field scanning optical microscopy with near-field probes (NSOM), the superoscillating mask will allow placing the object at a considerable distance from the mask. For many biomedical imaging applications, this is a crucial advantage over NSOM.

Regarding practical implementations of the superoscillating mask, the above calculations demonstrate that manufacturing tolerance should be of the order of 0.1λ. Thus, manufacturing such a phase mask from a slab of dielectric material for microwave and THz frequency focusing should not be a very challenging problem. It can then be covered with an absorbing film of variable thickness to create the desired transmission profile. Fabricating such a mask for the IR and optical parts of the spectrum presents a more significant challenge and a fabrication accuracy of between 5 and 50 nm will be required. However, even such challenging phase masks may be created from glass with the diamond milling techniques used to produce aspheric lenses, while further fine-tuning with true nanoscale resolution may be achieved using focusing ion beam milling. Here, the absorbing part of the mask could be a metal film of variable density prepared by UV or e-beam lithography.

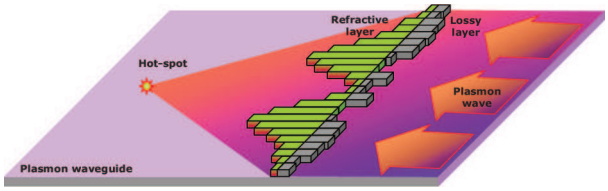

Figure 6. Plasmonic superoscillation focusing. A plasmonic mask is archived by placing a sculptured dielectric refractive layer on top of a flat metal surface to create the phase profile followed by a sculptured lossy layer to create the intensity profile.

The idea of superoscillation could also be applied to the creation of a superhigh-resolution plasmonic device. Surface plasmon-polaritons are collective oscillations of light and electrons that propagate along the interface between a metal (e.g., gold, silver) and a dielectric. They are essentially two-dimensional waves that can create complex field patterns by interference.[29,30] As plasmon wavelengths are somewhat shorter than those of light at the same frequency, plasmonic devices promise better resolution than optical devices even within the conventional Abbe−Rayleigh diffraction limit. We argue that this may be enhanced even further through the use of superoscillation as the approach developed above may be easily applied to plasmons. A possible implementation of a plasmonic focusing device is presented in Figure 6. Here, in order to create a desired intensity and phase profile of the mask we exploit the fact that the complex refractive index for plasmons depends on the dielectric properties ε of the medium forming an interface with the metal:[31] $\tilde{n} = ((\varepsilon_m \varepsilon)/(\varepsilon_m + \varepsilon))^{1/2}$. By preparing a film of lossless dielectric on a metal surface with a prescribed profile, one can create the desired phase profile for the plasmon mask. Using an additional lossy profiled dielectric layer on the top of the first, the necessary intensity profile can be engineered. Here, the transmission function of the surface plasmon mask should be derived taking account of losses (see Appendix, eq A7).

In summary, we have shown that an optical mask can be designed that creates a a subwavelength focus in an area beyond the evanescent fields. Such a mask may also be used as a super-resolution imaging device with numerous applications, for instance, for imaging inside a leaving cell, which is impossible with a near-field device.

Acknowledgment. We acknowledge the financial support of the Engineering and Physical Sciences Research Council, U.K.

Appendix A: Designing a Superoscillating Mask. Here, we describe a method to design a mask with a complex transmission function $t(x)$ that will generate a prescribed field distribution $f(x)$ within a limited region $[-D/2, D/2]$ at a distance z from the mask using prolate spheroidal wave functions.[26] We assume that the mask is illuminated at normal incidence with a plane monochromatic wave $E(x, z = 0) = 1$ (the time dependent factor $e^{i\omega t}$ is omitted) with a wavelength $\lambda = 2\pi/k_0$. In the scalar angular spectrum description of light propagation,[32] the field at a point (x, z) is

$$E(x,z) = \int_{-k_0}^{k_0} T(u) e^{iux} e^{iz\sqrt{k_0^2-u^2}} du \tag{A1}$$

where $T(u)$ is the Fourier transform of $t(x)$. We now approximate $h(x) \equiv E(x, z)$ as a limited series of orthogonal prolate spheroidal wave functions $\psi_n(c, x)$ that are band-limited to the frequency domain $[-k_0, k_0]$.

$$h_N(x) = \sum_{n=0}^{n=N} a_n(c)\psi_n(c,x) \tag{A2}$$

Here a_n depends on a constant $c = (\pi D)/(\lambda)$, and the Fourier transform function of $h_N(x)$ is given by

$$H_N(u) = \sum_{n=0}^{n=N} \frac{\pi a_n \psi_n\left(c, \frac{uD}{2k_0}\right)}{i^n R_{0n}^{(1)}(c,1)} \tag{A3}$$

where $R_{0n}^{(1)}(c, 1)$ is a radial prolate spheroidal wave function of the first kind, and

$$h_N(x) = \int_{-k_0}^{k_0} H_N(u) e^{iux} du \tag{A4}$$

Comparing eqs A1 and A4, we find that the required transmission function $t(x)$ of the mask is

$$t(x) = \sum_{n=0}^{n=N} \int_{-k_0}^{k_0} \frac{\pi a_n \psi_n\left(c, \frac{uD}{2k_0}\right)}{i^n R_{0n}^{(1)}(c,1)} e^{iux - iz\sqrt{k_0^2-u^2}} du \tag{A5}$$

It follows from the angular spectrum representation that to design a mask with a transmission function $m(x)$, which upon illumination by a point line object (located at a distance z_1 from the mask) will convert its divergent incident field into a prescribed field distribution $h(x)$ at a distance z from the other side of the mask, the following equation should be used:

$$m(x) = \frac{t(x)}{\int_{-k_0}^{k_0} e^{iux} e^{iz_1\sqrt{k_0^2-u^2}} du} \tag{A6}$$

$t(x)$ is given by eq A5. In the case of the lossy medium, the transmission function $A(5)$ shall be corrected:

$$t(x) = \sum_{n=0}^{n=N} \int_{-|k_0|}^{|k_0|} \frac{\pi a_n \psi_n\left(c, \frac{uD}{2|k_0|}\right)}{i^n R_{0n}^{(1)}(c,1)} e^{zIm[\sqrt{k_0^2-u^2}]} \times e^{iux - iz\mathrm{Re}[\sqrt{k_0^2-u^2}]} du \tag{A7}$$

where k_0 is a complex wave-vector in the lossy medium.

References

(1) Betzig, E.; Trautman, J. K.; Harris, T. D.; Weiner, J. S.; Kostelak, R. L. *Science* **1991**, *251*, 1468–1470.
(2) Hartschuh, A.; Sanchez, E. J.; Xie, X. S.; Novotny, L. *Phys. Rev. Lett.* **2003**, *90*, 095503.
(3) Li, K.; Stockman, M. I.; Bergman, D. J. *Phys. Rev. Lett.* **2003**, *91*, 227402.
(4) Stockman, M. I. *Phys. Rev. Lett.* **2004**, *93*, 137404.
(5) Merlin, R. *Science* **2007**, *317*, 927–929.
(6) Grbic, A.; Jiang, L.; Merlin, R. *Science* **2008**, *320*, 511–513.
(7) Pendry, J. B. *Phys. Rev. Lett.* **2000**, *85*, 3966–3969.
(8) Durant, S.; Liu, Z.; Steele, J. M.; Zhang, X. *J. Opt. Soc. Am. B* **2006**, *23*, 2383–2392.
(9) Salandrino, A.; Engheta, N. *Phys. Rev. B* **2006**, *74*, 075103.
(10) Jacob, Z.; Alekseyev, L. V.; Narimanov, E. *Opt. Exp.* **2006**, *14*, 8247–8256.
(11) Fang, N.; Lee, H.; Sun, C.; Zhang, X. *Science* **2005**, *308*, 534–537.

(12) Liu, Z.; Durant, S.; Lee, H.; Pikus, Y.; Fang, N.; Xiong, Y.; Sun, C.; Zhang, X. *Nano Lett.* **2007**, *7*, 403–408.
(13) Liu, Z.; Lee, H.; Xiong, Y.; Sun, C.; Zhang, X. *Science* **2007**, *315*, 1686.
(14) Toraldo Di Francia, G. 1952, *9*, 426−438.
(15) Berry, M. V.; Popescu, S. *J. Phys. A: Math. Gen.* **2006**, *39*, 6965–6977.
(16) Aharonov, Y.; Anandan, J.; Popescu, S.; Vaidman, L. *Phys. Rev. Lett.* **1990**, *64*, 2965–68.
(17) Ferreira, P. J. S. G.; Kempf, A. *IEEE Trans. Signal Process* **2006**, *54*, 3732–40.
(18) Tollarksen, J. *J. Phys: Conf. Ser.* **2007**, *70*, 012016.
(19) Huang, F. M.; Chen, Y.; Garcia de Abajo, F. J.; Zheludev, N. I. *Appl. Phys. Lett.* **2007**, *90*, 091119.
(20) Huang, F. M.; Chen, Y.; Garcia de Abajo, F. J.; Zheludev, N. I. *J. Opt. A: Pure Appl. Opt.* **2007**, *9*, S285−S288.
(21) Tsukerman, I. *arXive:0811.2247v1*; 2008.
(22) Oseen, C. W. *Annalen. der. Physik.* **1922**, *374*, 202.
(23) Schelkunoff, S. A. *Bell. Syst. Techn. Journ.* **1943**, *22*, 80.
(24) Bouwkamp, C. J.; Bruijn, N. G. *Philips. Res. Rep.* **1946**, *1*, 135.
(25) Woodward, P. M.; Lawson, J. D. *J. I. E. E.* **1948**, *95*, 363.
(26) Slepian, D.; Pollak, H. O. *Bell System Tech. J.* **1961**, *40*, 44–63.
(27) Huang, F. M.; Kao, T. S.; Fedotov, V. A.; Chen, Y.; Zheludev, N. I. *Nano Lett.* **2008**, *8*, 2469–2472.
(28) Born, M.; Wolf, E. *Principles of Optics*, 2nd ed.; 1964; p 334.
(29) Dennis, M. R.; Zheludev, N. I.; Garcia de Abajo, F. J. *Opt. Exp.* **2007**, *15*, 9692–9700.
(30) Krenn, J. R.; Weeber, J.-C. *Philos. Trans. R. Soc. London, Ser. A* **2004**, *362*, 739–756.
(31) Zayats, A. V.; Smolyaninovb, I. I.; Maradudinc, A. A. *Phys. Rep.* **2005**, *408*, 131–314.
(32) Mandel L.; Wolf E. *Optical Coherence and Quantum Optics*; Cambridge University Press: New York, 1995.

NL9002014